JOURNAL OF MATERIALS SCIENCE 30 (1995) 6171–6178

Kinetic behaviour and reactivity of zinc ferrites for hot gas desulphurization

M. PINEDA, J. L. G. FIERRO, J. M. PALACIOS*
Instituto de Catálisis y Petroleoquímica, Campus Universidad Autónoma, Cantoblanco, 28049 Madrid, Spain

C. CILLERUELO, J. V. IBARRA
Instituto de Carboquímica, Poeta Luciano Gracia 15, 50015 Zaragoza, Spain

Different zinc ferrite samples have been prepared with varying Fe:Zn atomic ratios and preparation procedures in order to optimize their behaviour as hot gas desulphurization agents. Kinetic studies on metal oxide sulphidation were performed in a thermobalance and sulphur removal tests were conducted in a fixed-bed reactor. Fresh and exhausted samples were characterized by several physical techniques. The results show that reaction rate is mainly controlled by mass transfer processes of the reactant through the gas film in contact with the solid and through the sulphide layer. Bulk ferrites displayed the best performance for sulphur removal. Ferrites deposited on an alumina substrate by impregnation are highly dispersed, however they exhibited a very poor efficiency for sulphur removal. Solid-state reactions of single oxides at the alumina interface, i.e. zinc and/or iron aluminate formation, instead of pore occlusion by the active ingredient seem to be responsible for a low reactivity.

1. Introduction

Emerging technologies for a more efficient coal gasification, such as integrated gasification combined-cycle power generation (IGCC) [1], employing gas turbines and gasifier molten carbonate fuel cells (MCFC) [2], power plants, together with more and more severe environmental regulations require gas clean-up to attain sulphur levels < 10 p.p.m. There is experimental evidence to suggest that such levels can be reached by passing hot gases through a metal-oxide bed. The H_2S present in the gas stream reacts with the metal oxide to form the sulphide, thus being trapped by chemical reaction. The overall process includes: (1) some reduction prior to sulphidation in those locations of the bed far from the inlet; (2) sulphidation of metal oxide until the H_2S level in the outlet becomes high; (3) regeneration of the sulphided material without significant mechanical strength losses.

For their high conversion and low cost, iron oxides were the first materials investigated. However, they suffer from the high temperatures of the process. Temperatures above 400 °C have to be avoided because they are easily reduced with subsequent losses in efficiency [3, 4] and rapid sintering in the regeneration step. For an efficient power generation, desulphurization has to occur in the temperature range 650–800 °C. Higher operation temperature and higher efficiency in sulphidation can be obtained with zinc oxide [5]. Zinc and iron mixed oxides (ferrites) are more stable, allowing extension of the temperature range up to 600 °C [6]. Several unresolved problems still reside in using zinc ferrites: (1) when the H_2S concentration in the outlet gas becomes high (for instance, > 100 p.p.m.), sulphur removal reaches only 40–50% of the theoretical value; (2) if a threshold temperature is surpassed, ferrite decomposes into the individual oxides which, in turn, are easily reduced to the metals (metallic zinc is lost by evaporation); (3) the high stability of zinc sulphate requires somewhat higher regeneration temperatures than sulphidation, with the subsequent efficiency loss and irreversible damage by sintering. Accordingly, new metal oxides, such as those of Ti, Mn, Cu, Ce and Sn [1, 7–9] have been proposed as candidates, although their development has been rather scant.

Concerning the sulphidation process, kinetic studies on ferrites showed that, on the one hand, the reaction rate is mainly controlled by diffusional transport, as revealed by the small effect of temperature over the range 500–700 °C, and the large influence of particle size [10]. On the other hand, important chemical and structural changes, induced by sulphide nucleation and sintering, occur during sulphidation [11]. Consequently, the performance of ferrites can be greatly altered by changing the preparation, because both structure and phase distribution strongly depend on the genesis of the mixed oxide. A few studies have focused on the relevance of the shape, composition, dispersion, etc., on the performance. However, such studies have been directed toward the development of

*Author to whom all correspondence should be addressed.

0022–2461

more reactive substrates with higher mechanical strength in order to be used in fluidized [12] or mobile-bed reactors [13]. Apart from this, there is lack of precise characterization of the fresh and spent materials, and the effect of the parameters studied on the reactivity is not well understood.

The aim of the present work is to study the desulphurization process on various zinc ferrites prepared by different methods with Fe:Zn ratios ranging between 0.8 and 1.2. By combining both the performance and properties of the fresh and spent materials, as revealed by physical techniques, an attempt to optimize the performance of these oxides is made.

2. Experimental procedures

2.1. Materials

Four types of samples were prepared (Table I). Type I samples were prepared by calcination of commercial bulk oxides (Merck, reagent grade). Type 2 samples were similar to their type 1 counterparts, although after calcination they were mixed in the proportion 10:90 with Al_2O_3 (Girdler Sud-Chemie, S_{BET} = 188 m^2 g, particle diameter = 0.4–0.6 mm). Types 3 and 4 were prepared by impregnation of Al_2O_3 with aqueous solutions of $Zn(NO_3)_2$ and $Fe(NO_3)_3$ (Merck, reagent grade) of the appropriate concentrations to obtain a given percentage and Fe:Zn atomic ratio. As the impregnation was in excess solution, water was removed in a rotary evaporator at 65 °C, the samples were then dried overnight at 120 °C. All samples were finally calcined at 650 °C for 16 h. Three samples with Fe:Zn ratios varying between 0.8 and 1.2 were included in each type. Labelling and composition of the samples is compiled in Table I.

2.2. Desulphurization tests

The kinetics of desulphurization were performed on 10 mg samples using a Setaran TGD TA92 thermogravimetric analyser under isothermic conditions, which were specific for a given experiment. Activity tests were conducted in a 1 cm i.d. stainless steel fixed-bed vertical microreactor, including two sections for preheating and reaction, respectively. Gas analyses at the inlet and outlet were performed by mass spectrometry using a quadrupole mass analyser. A 2 g sample, corresponding to a bed depth of 3.8 cm, was used in the experiments. The reaction conditions were: total gas flow, 70 $cm^3 min^{-1}$; gas composition, 0.5 vol % H_2S and 99.5 vol % N_2; temperature, 540 °C; atmospheric pressure. Gases other than H_2S and N_2, such as H_2, CO, CO_2 and H_2O, present at the outlet of a coal gasifier, were not introduced.

2.3. Characterization techniques

The N_2 isotherms were measured at 77 K using Micromeritics ASAP-2000 equipment. Pore-volume distributions were obtained by Hg intrusion with a Micromeritics pore sizer 9310 instrument up to a final pressure of 2.1×10^7 Pa, which allowed filling of pores down to 3 nm diameter. The X-ray diffraction patterns were recorded using a Seifert 3000 diffractometer using nickel-filtered CuK_α radiation.

Morphological studies and element distributions were carried out with a SEM–EDX equipment consisting of an ISI DS-130 scanning electron microscope coupled to a Si(Li) X-ray detector and a Kevex 8000II processor for energy-dispersive X-ray analysis. Photoelectron spectra were acquired with a Fisons ESCALAB MkII 200R spectrometer equipped with a hemispherical electron analyser and a MgK_α 120 W X-ray source. A PDP 11/04 computer from Digital Equipment Co. was used for collecting and analysing the spectra. The pressure in the ion-pumped analysis chamber was maintained below 2.0×10^{-7} Pa during data acquisition. The spectra were collected for 20–90 min, depending on the peak intensities, at a pass energy of 20 eV, which is typical in high resolution conditions. Curve deconvolution procedures using Lorentzian/Gaussian mix were employed for peak area measurements. All binding energies (BE) were referenced to the C1s line at 284.9 eV. This reference gave BE values with an accuracy of $\pm$ 0.2 eV.

3. Results and discussion

3.1. Characterization of fresh samples

The FeK_α and ZnK_α SEM–EDX line profiles for a representative pellet sample before and after calcining are displayed in Fig. 1a and b, respectively. Before

TABLE I Labelling and preparation methods of samples

Type	Sample	Dispersant or support (wt %)	Preparation method
1	FZ(1:1.2) M FZ(1:1) M FZ(1:0.8) M	None	Physical mixture of bulk oxides and further calcination
2	FZ(1:1.2) A90M FZ(1:1) A90M FZ(1:0.8) A90M	γ-Al_2O_3 (90) d_p = 0.4–0.6 mm	Type 1 diluted in γ-Al_2O_3 90 wt %
3	FZ(1:1.2) A90I FZ(1:1) A90I FZ(1:0.8) A90I	γ-Al_2O_3 (90) d_p = 0.4–0.6 mm	Impregnation of soluble salts and further calcination
4	FZ(1:1.2) A90I′ FZ(1:1) A90I′ FZ(1:0.8) A90I′	γ-Al_2O_3 (90) d_p < 0.2 mm	Similar to type 3 but with different particle size

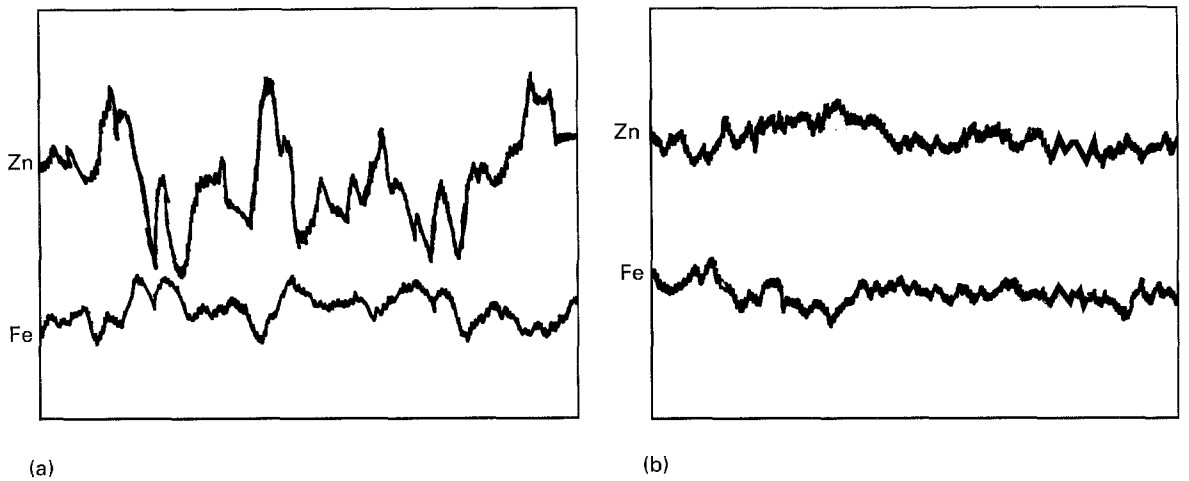

Figure 1 SEM–EDX FeK_α and ZnK_α line profiles from a mixture of oxides. (a) Before calcination; (b) after calcination at 650 °C for 16 h.

calcining, as the sample was a physical mixture of Fe and Zn oxides with particle sizes in the region 1–2 μm, the distribution of the elements was heterogeneous. These oxides were identified by XRD as α-Fe_2O_3 (hematite) and ZnO (zincite). However, upon calcining at 650 °C for 16 h (Fig. 1b) it appeared much more homogeneous due to solid-state reactions between Fe and Zn oxides yielding $ZnFe_2O_4$ (franklinite). Considering that thermodynamics is favourable for spinel formation under these experimental conditions, the reaction was not complete even when starting with stoichiometric ratios of $ZnO:Fe_2O_3$. The observation of small amounts of the individual ZnO and Fe_2O_3 oxides, whose proportion depends on the starting $ZnO:Fe_2O_3$ ratio, may be due to the diffusionally-controlled solid-state reaction rate between these oxides. The formation of crystalline phases are very clear for type 1 and 2 samples, however, the absence of diffraction patterns for type 3 and 4 samples suggests a high dispersion of these oxides on the alumina surface.

Table II gives the textural parameters for fresh samples. Type 1 samples displayed relatively low surface areas and pore volumes, corresponding to large pore sizes. On the contrary, type 3 and 4 samples exhibited large surface areas and pore volumes with very small pore sizes, which are associated with the alumina substrate. It is worth noting the larger porosity of the impregnated samples with greater particle sizes. Type 2 samples were intermediate with BET areas similar to those for the impregnated ones. The SEM micrographs showing the most characteristic morphological features of the samples are presented in Fig. 2. Bulk samples (type 1) consisted of aggregates of very small particles with porosity associated mainly with the interparticular voids (Fig. 2a). However, the impregnated samples (types 3 and 4) were built of large alumina particles on which the active ingredient was spread with a high degree of dispersion. Type 2 samples exhibited an intermediate situation with large alumina particles and small zinc ferrite particles deposited on them (Fig. 2b).

Photoelectron spectroscopy was used to determine the chemical state of the samples before and after calcination. The BE of core electrons are given in Table III. BE values at 1021.8–1022.6 and 710.3–711.7 eV for $Zn2p_{3/2}$ and $Fe2p_{3/2}$ levels, respectively, indicate the presence of Zn^{2+} and Fe^{3+} species. The large changes in BE of Fe2p peaks suggest the formation of new iron-containing oxide phases with the alumina substrate during calcination. Before calcining, the BE of the $Zn2p_{3/2}$ peak in impregnated samples was slightly higher than in the bulk counterparts, and the same tendency, but much more marked, was observed for the $Fe2p_{3/2}$ peak. This finding suggests that in the impregnated samples there is, even before calcining, interaction of the precursor with the alumina carrier. In addition to textural differences, XPS data provided support for dissimilarities in structure and chemical state of Fe and Zn between bulk and impregnated samples. In addition, the Fe:Zn atomic ratio (Table IV), calculated from the experimental intensities and published sensitivity factors, indicated Fe enrichment at the surface, suggesting that ferrite formation is a less favoured process when Al_2O_3 is present.

The stability of the adsorbents against reduction by the gas stream coming from coal gasification is an extremely useful property, so that the adsorber layers placed far enough from the reactor inlet are subjected, for a given time, to the reducing action of the clean

TABLE II Textural parameters of fresh samples

Type	Sample	S_{BET} ($m^2\,g^{-1}$)	V_p ($cm^3\,g^{-1}$)	D_p (nm)
1	FZ(1:1) M	81	0.28	8.2
2	FZ(1:1.2) A90M	162	0.37	7.6
	FZ(1:1) A90M	165	0.48	7.2
	FZ(1:0.8) A90M	175	0.39	7.2
3	FZ(1:1.2) A90I	166	0.76	6.8
	FZ(1:1) A90I	167	0.79	6.8
	FZ(1:0.8) A90I	168	0.42	6.8
4	FZ(1:1.2) A90I′	164	0.50	6.9
	FZ(1:1) A90I′	166	0.52	6.8
	FZ(1:0.8) A90I′	164	0.50	6.9

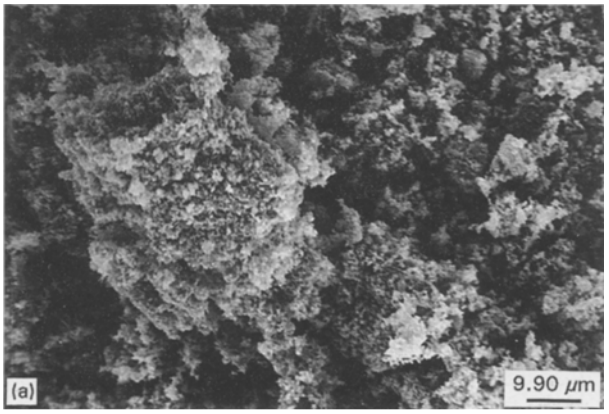

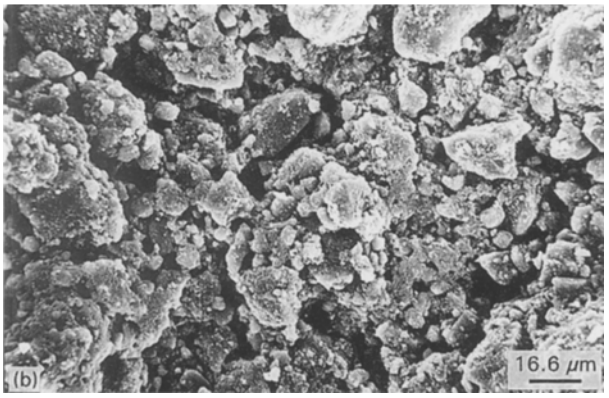

Figure 2 Morphological appearance of a mixture of oxides after calcination at 650 °C for 16 h. (a) Sample FZ(1:0.8)M; (b) sample FZ(1:1)A90M.

TABLE III Binding energies (eV) of $Zn2p_{3/2}$ and $Fe2p_{3/2}$ core electrons for fresh samples before and after calcination

Sample	Before calcination		After calcination	
	$Zn2p_{3/2}$	$Fe2p_{3/2}$	$Zn2p_{3/2}$	$Fe2p_{3/2}$
FZ(1:1) M	1022.2	710.3	1021.8	711.0
FZ(1:1) A90I	1022.3	710.7	1022.4	711.3
FZ(1:1) A90I'	1022.6	711.1	1022.4	711.7

gases once they became desulphided at the inlet. If this is the case, ferrite will be decomposed to its oxide components and then reduced as separate phases. The kinetics of the process has been reported to be strongly influenced when lower oxidation states are reached [6], and in the case of Zn additional losses by evaporation may also occur. TPR profiles for type 1 samples are shown in Fig. 3. These profiles display two reduction steps: the first at ca. 450 °C, whose weight loss corresponds to reduction of Fe_2O_3 to Fe^0, and the second at ca. 675 °C associated with reduction of ZnO to Zn and the subsequent evaporation of metallic Zn. From these results, it appears that in a reducing atmosphere the $ZnFe_2O_4$ compound decomposes into ZnO and Fe_2O_3 oxides, which then reduce independently. This finding indicates that zinc ferrite formation does not contribute to stabilization in a hydrogen environment in agreement with [8]. Similar TPR experiments were performed on the impregnated samples, however, in no cases were TPR peaks observed over the whole temperature range, confirming the XPS findings on the formation of metal aluminates at the alumina interface.

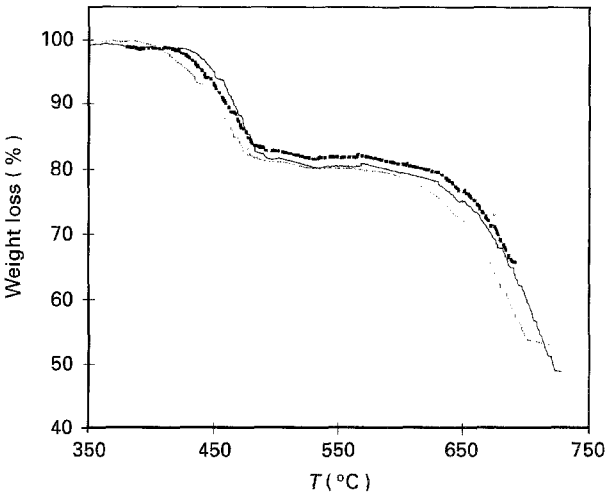

Figure 3 Temperature-programmed reduction profiles of Zn ferrites with different compositions: 50 $cm^3 min^{-1}$, 25 vol % H_2, 75 vol % He. ....., FZ(1:0.8)M; ———, FZ(1:1)M; ■ ■, FZ(1:1.2)M.

3.2. Reactivity tests

Kinetic data for sulphiding of the FZ(1:1)M sample are displayed in Figs 4 and 5. The effect of gas phase H_2S concentration on the kinetics of sulphiding is illustrated in Fig. 4. It is clear that the sulphiding rate increases proportionally with the H_2S concentration (first-order reaction), whereas the time required to achieve equilibrium follows the opposite trend. The absence of significant temperature effects on the kinetics (Fig. 5) suggests the process to be mainly controlled by the H_2S transport into and across the interface. It has been reported that the sulphidation process can be

TABLE IV XPS atomic ratio in impregnated samples before and after calcination

Sample	Before calcination			After calcination		
	Zn/Al	Fe/Al	Fe/Zn	Zn/Al	Fe/Al	Fe/Zn
FZ(1:1.2) A90I	0.034	0.048	0.88	0.013	0.012	0.58
FZ(1:1) A90I	0.033	0.059	1.12	0.010	0.020	1.13
FZ(1:0.8) A90I	0.027	0.052	1.19	0.009	0.022	1.50
FZ(1:1.2) A90I'	0.034	0.075	1.37	0.014	0.026	1.12
FZ(1:1) A90I'	0.032	0.062	1.22	0.013	0.030	1.44
FZ(1:0.8) 90I'	0.025	0.063	1.57	0.012	0.025	1.31

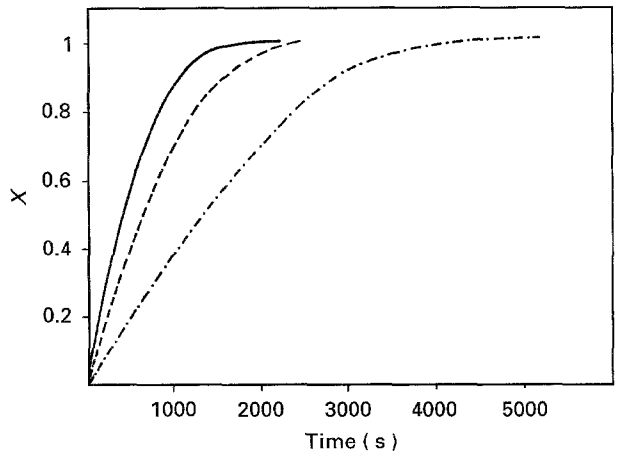

Figure 4 Microgravimetric study of the sulphurization of sample FZ(1:1)M at 500 °C as a function of the H_2S concentration. ———, 1.5% H_2S; – – –, 1% H_2S; – · – · –, 0.5% H_2S.

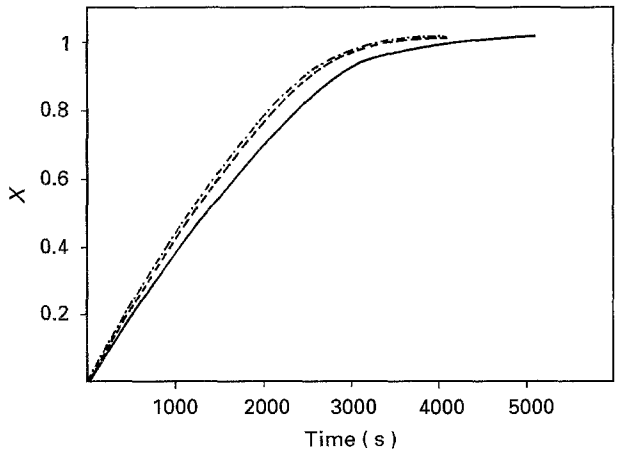

Figure 5 Microgravimetric study of the sulphurization of sample FZ(1:1)M as a function of temperature at constant H_2S concentration (0.5% H_2S). Temp. (°C): ——, 540; – – –, 600; – · – · –, 650.

accurately described by the shrinking model [6, 10, 13], which predicts the solid conversion, X, with time, t, for on-stream cylindrical particles

$$t = A_1X + A_2[X + (1 - X)\ln(1 - X)] + A_3[1 - (1 - X)^{1/2}] \quad (1)$$

The first term on the right-hand side of Equation 1 corresponds to transport of H_2S through the gas film, the second represents the H_2S diffusion across the formed sulphide shell and the third the intrinsic reaction term. The parameters A_1, A_2 and A_3 have been evaluated by multiple-regression analysis. The best fit with experimental results was obtained by omitting the third term in Equation 1, thus confirming the above assumption that the intrinsic reaction rate is very high and the process is exclusively controlled by transport phenomena. For instance, by considering only the first two terms of Equation 1, the correlation coefficient is better than 0.99, and sometimes even better than 0.999. The A_1 and A_2 values calculated for the bulk FZ(1:1)M and FZ(1:0.8)M samples under different reaction conditions are summarized in Table V. As expected, both A_1 and A_2 become affected by the H_2S concentration to the same extent, however, particle size and temperature have a much larger influence on A_2 than on A_1. The sample with the stoichiometric ferrite composition displays higher A_2 values, which implies smaller diffusion coefficients.

Fig. 6 displays the breakthrough curves obtained with the fixed-bed reactor for the four samples possessing molar ratios of 1: 1. All these curves are similar, the H_2S concentration at the outlet is very low, however after a certain elapsed time the breakthrough occurs and this increases drastically to almost the same level as that in the inlet. The breakthrough time, as defined by the point at which a rapid increase in the H_2S concentration occurs, differs from sample to sample. Thus, this time is 2240 min for the FZ(1:1)M sample, 202 min for the FZ(1:1)A90M sample (with ca. 1/10 of the active oxide) and ca. 22 and 9 min for the FZ(1:1)A90I and FZ(1:1)A90I′ samples, respectively. The latter two have the same proportion of metal oxide as the FZ(1:1)A90M sample. As all these curves increase rapidly with the same profile; it therefore appears that the reaction rate is very similar for the impregnated and bulk samples. The poor behaviour of the impregnated samples appears to be due more to the rapid exhaustion of the active oxide than to diffusional problems appearing by plugging-up of pores. A similar finding was reported by Gupta *et al.* [12], using a bench-scale reactor and working with ferrites prepared by different routes. The samples

TABLE V Sulphiding reaction in thermobalance. Best-fit parameters A_1 and A_2 obtained using the unreacted core model

Sample	$2R \times 10^{-4}$ (cm)	$C_{H_2S} \times 10^{-6}$ (mol cm^{-3})	T (°C)	Flow rate (cm^3 s^{-1})	$A_1 \times 10^3$ (s)	$A_2 \times 10^3$ (s)
FZ(1:1) M	400	7.5	540	2.33	1.87	2.10
	400	7.5	600	2.33	1.92	1.48
	400	7.5	650	2.33	2.13	1.23
	400	15.0	540	2.33	0.90	1.15
	400	22.5	540	2.33	0.45	1.07
FZ(1:0.8) M	50	7.5	540	1.67	2.36	0.56
	50	7.5	540	3.33	2.35	1.10
	50	7.5	540	5.00	2.11	1.33
	100	7.5	540	3.33	2.34	1.20
	200	7.5	540	3.33	2.61	0.88
	320	7.5	540	3.33	2.42	0.79
	400	7.5	540	3.33	2.33	1.81

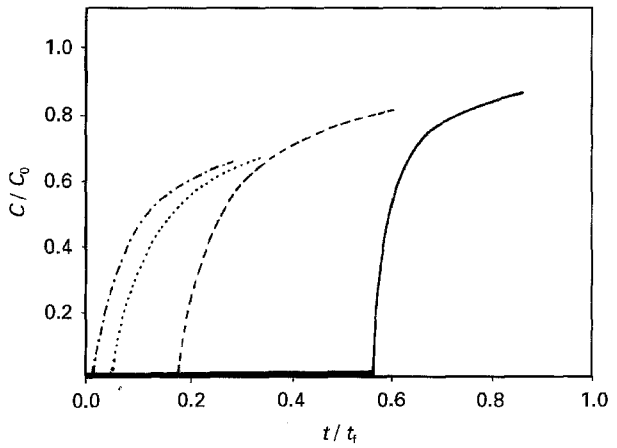

Figure 6 Breakthrough curves in the sulphurization reaction for the 1:1 molar ratio Zn ferrite. ——, FZ(1:1)M; – – –, FZ(1:1)A90M; ...., FZ(1:1)A901; – · – ·; FZ(1:1)A90I'.

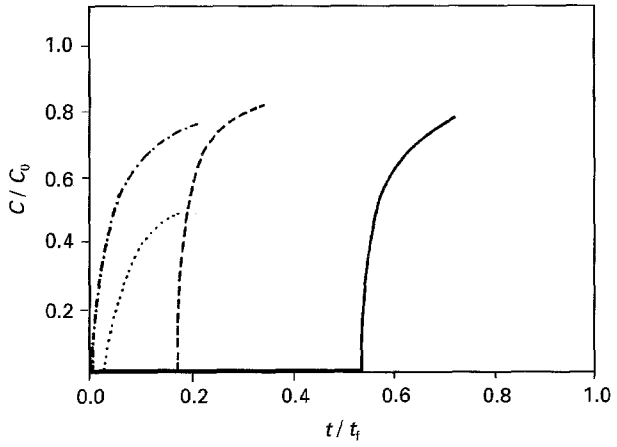

Figure 7 Breakthrough curves in the sulphurization reaction for the 1:1.2 molar ratio Zn ferrite. ——, FZ(1:1.2)M; – – –, FZ(1:1.2)A90M; ...., FZ(1:1.2)A90I; – · – ·, FZ(1:1.2)A90I'.

prepared by impregnation exhibited a low sulphidation capability but no explanation was advanced. In our case, the data in Fig. 6 suggest that most of the Zn and Fe oxides in the impregnated samples remained inactive, with only a small fraction of the oxides being sulphidable. Identical breakthrough curves (Fig. 7) have been obtained for the samples with the molar ratio (1:1.2). Again, the samples prepared by impregnation displayed a much lower capacity for H_2S retention than expected taking into account that the Zn and Fe concentrations were similar to that of sample FZ(1:1.2) A90M. Again, the slope of the breakthrough curves also suggests that the abnormal behaviour of impregnated samples does not reside in the diffusional problems induced by the occlusion of the pores. The breakthrough times appear almost independent of the molar ratio of the oxide components used in the sample preparation (similar curves in Figs 6 and 7).

3.3. Characterization of sulphided samples

The sulphur content, as measured by elemental analysis (EA) and EDX, and the crystalline phases identified by XRD in sulphided samples after completion of the sulphidation test are compiled in Table VI. As can be seen, the ZnS (sphalerite) and $Fe_{1-x}S$ (pyrrhotite) are clearly identified in the bulk samples. The formation of these compounds implies strong structural and morphological changes of the precursor oxides derived from segregation of the metal oxide constituents of the original ferrite and their further nucleation, and even sintering, into the respective sulphides. The absence of crystalline phases other than that of the γ-Al_2O_3 in the sulphided samples prepared by impregnation indicates a very high degree of dispersion of the metal sulphides.

TABLE VI Sulphur concentration and crystalline phases in sulphided samples

Sample	S concentration (wt %) EDX	EA	Calc.	Phases identified by XRD
FZ(1:1.2) M	33.7	32.4	35	ZnS, $Fe_{(1-x)}S$
FZ(1:1.2) A90M	9.1	4.4	3.5	γ-Al_2O_3, ZnS, $Fe_{(1-x)}S$
FZ(1:1.2) A90I	6.2	0.7	3.5	γ-Al_2O_3
FZ(1:1.2) A90I'	9.5	–	3.5	γ-Al_2O_3

The amount of sulphur retained by sample FZ(1:1.2)M, as evaluated by EDX and elemental analysis, agrees reasonably well with that expected for the complete conversion of the $ZnFe_2O_4$ ferrite into the stoichiometric Zn and Fe sulphides. For the bulk sample physically mixed with alumina, the chemical analysis by EDX differs substantially from that by EA. While the sulphur content measured by EA almost coincides with the calculated sulphur content, the value obtained by EDX is much greater. The explanation of this lies in the fact that S-containing phases are dispersed in the form of small particles on larger alumina ones, and therefore an essentially surface technique such as EDX overestimates the sulphur present in this sample. Sulphur analyses for the impregnated samples also showed quite dissimilar results. Firstly, the sulphur content as evaluated by EA is substantially smaller than that calculated assuming complete sulphidation, suggesting partial transformation of the oxidic precursors during the sulphidation process. Secondly, the sulphur content measured by EDX is much larger than that provided by chemical analysis, implying, as advanced above, that the sulphide phase is accumulated on the surface of the alumina particles.

The textural properties of sulphided samples are summarized in Table VII. A comparison of these properties with that of the calcined homologous (Table II) indicates important changes induced by sulphidation. Sulphidation led to a dramatic change, almost one order of magnitude, in the BET area of bulk samples, although the decrease in the pore volume and the parallel increase in pore diameter were small. This means that the smaller particles of the original Zn and Fe oxides disappeared in the course of sulphidation and built-up into larger metal sulphide structures. Similar effects were observed in the physically mixed alumina and metal oxides, although the changes were less drastic because only one-tenth of the metal oxide was present with respect to the bulk

TABLE VII Textural properties of sulphided samples

Sample	S_{BET} ($m^2\ g^{-1}$)	V_p ($cm^3\ g^{-1}$)	D_p (nm)
FZ(1:1.2) M	11	0.31	8.7
FZ(1:1.2) A90M	139	0.51	7.5
FZ(1:1.2) A90I	152	0.68	6.9
FZ(1:1.2) A90I′	151	0.77	6.9

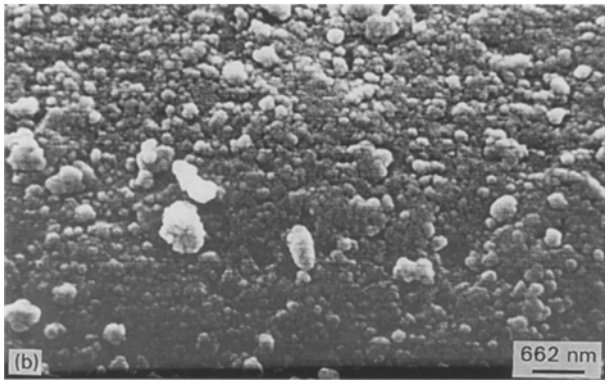

Figure 8 Morphological appearance of sulphided ferrites. (a) Sample FZ(1:1.2)M; (b) sample FZ(1:1.2)A90I.

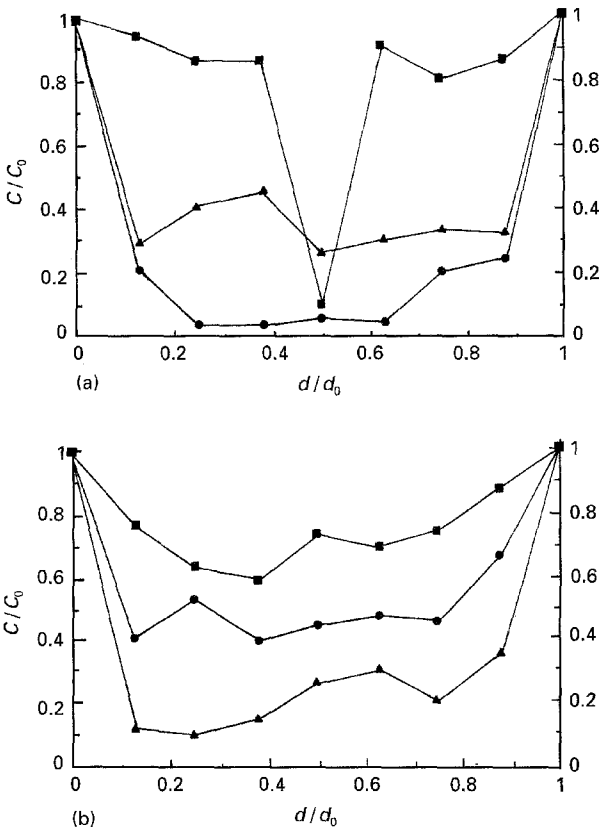

Figure 9 S, Fe and Zn concentration profiles on a cross-section of sulphided samples prepared by impregnation. (a) sample FZ(1:1.2) A90I; (b) sample FZ(1:1.2)A90I′. ▲, S; ●, Fe; ■, Zn.

samples. Finally, the change in the textural properties was very small for the impregnated samples, suggesting that no pore occlusion took place during the incorporation of Fe and Zn. Accordingly, the low efficiency of the impregnated samples can be associated not only to the low metal content but to the chemical state and/or the Fe and Zn distribution within the alumina particles.

Evidence on the morphological changes brought about by the desulphurization process in the bulk and impregnated samples is shown in Fig. 8. Fig. 8a shows that the particle size of the resulting sulphides is 0.2–0.3 μm, much larger than that of the original ferrite. This may explain the significant decrease in surface area and the moderate decay of porosity, the pores being mainly associated with interparticular void volume. The impregnated sample (Fig. 8b) shows a layer of particles, mainly of pyrrhotite, covering the alumina surface, whereas zinc sulphide is less abundant on the outer surface.

The distribution of S, Fe and Zn elements across the diameter of a cross-section of a sulphided alumina particle has been obtained through local analysis by EDX. These results are illustrated in Fig. 9a and b. Zn distribution is rather uniform, whereas Fe is mainly concentrated on the outer surface of the alumina particles. According to these quite dissimilar distributions of Fe and Zn, it is highly unlikely that a zinc ferrite would be present in calcined samples. Therefore, it can be reasonably inferred that the impregnation and calcination steps determine, to a great extent, the element distribution. This apparent Fe enrichment of the surface in the impregnated samples is in good accordance with the XPS data (Table IV). Another important finding to be noted is the location of sulphur essentially on the external surface of the alumina particles. Since the Zn is almost uniformly distributed, it can be concluded from EDX data that most of the Zn remains unsulphided.

Additional information on the chemical state of the elements at the sample surface comes from the photoelectron spectra. Table VIII summarizes the BE of $Zn2p_{3/2}$, $Fe2p_{3/2}$ and $S2p_{3/2}$ peaks. For the $Zn2P_{3/2}$ peak, two contributions at ca. 1021.0 eV, associated with Zn sulphide species, and at 1022.5–1023.3 eV, ascribed to non-sulphided Zn^{2+} ions in an oxygen environment, are observed. Similarly, the $Fe2p_{3/2}$ peak exhibited two contributions at ca. 709.1 eV, whose origin lies in the Fe sulphide, and at 710.3–710.9 eV associated with non-sulphided (oxidic) Fe species, such as those present in Fe aluminate or sulphate. Finally, the observation of two S2p peaks at 161.3 and 168.5–169.3 eV leads to the conclusion that

TABLE VIII Binding energies (eV) of core electrons in sulphided samples

Sample	$Zn2p_{3/2}$	$Fe2p_{3/2}$	$S2p_{3/2}$
FZ(1:1.2) M	1021.0	709.1	161.3
	1022.5	710.9	163.9
			168.5
FZ(1:1.2) A90M	1022.0	710.3	161.1
	1023.3		
FZ(1:1.2) A90I	1022.8	710.9	161.0
			169.3
FZ(1:1.2) A90I'	1022.7	710.8	169.3

sulphide ions (peak at 161.3 eV) become partially oxidized upon exposure to air according to the reaction: $S^{2-} + 2O_2 \rightarrow SO_4^{2-}$; the resulting sulphate ions being bonded to Al^{3+} or Fe^{3+}/Fe^{2+} ions.

Surface analysis indicated, in agreement with XRD data, that sulphided FZ(1:1.2)M and FZ(1:1.2)A90M samples display Zn sulphide (sphalerite) and Fe sulphide (pyrrhotite) as the major phases with minor amounts of Zn and Fe sulphates. As these later phases cannot be detected by the XRD technique, it can be inferred that they are a few layers thick and that they are formed by oxidation of the sphalerite and pyrrhotite phases upon exposure to air. The observation of the $Zn2p_{3/2}$ BE at 1023.3 eV for the sample FZ(1:1.2) A90 can be taken as conclusive of a strong interaction of Zn oxide with the alumina surface. Finally, it must be stressed that S, Fe and Zn atoms are placed in an oxygen environment for the impregnated samples, indicating a very small degree of sulphidation which almost disappears upon air exposure.

4. Conclusions

In order to improve the performance in the desulphurization process of hot gases and/or to increase the mechanical strength, Zn ferrites have to be prepared mixed with inactive materials, such as bentonites, silica, alumina, etc. Zn ferrites prepared using different methods and compositions have been tested in the desulphurization of hot gases. The Fe:Zn ratio was varied in the range 0.80–1.20 and the extent of formation of the $ZnFe_2O_4$ ferrite was not complete even in the Fe:Zn stoichiometric compositions. The kinetics of sulphidation of the samples can be reasonably described by the unreacted shrinking core model and the reaction rate is mostly controlled by the mass transport processes of H_2S from the gas phase and across the sulphide shell towards the interface. Fixed-bed reaction experiments led to the conclusion that the performance of the ferrites depends strongly on the preparation method. Longer breakthrough times and higher efficiencies were obtained with bulk materials. However, the impregnated samples displayed a poorer performance due to a less homogeneous distribution of the elements and a stronger interaction with the substrate, which makes only a small fraction of the oxides active.

Acknowledgement

This research was supported by the CECA under Contract 7220-EC/027.

References

1. K. V. THAMBIMUTHU, "Gas cleaning for advanced coal-based power generation", IEACR/53 (IEA Coal Research, London, March 1993) p. 97.
2. D. H. SCOTT, "Advanced power generation for fuel cells: implications for coal", IEACR/59 (IEA Coal Research, London, July 1993) p. 5.
3. E. SASAOKA, T. ICHIO and S. KASAOKA, *Energy and Fuels* **6** (1992) 603.
4. S. S. TAMHANKAR, M. HASATANI and C. Y. WEN, *Engng. Sci.* **36** (1981) 1181.
5. E. A. EFTHIMIADIS and S. V. SOTIRCHOS, *Chem. Engng. Sci.* **48** (1993) 1971.
6. G. D. FOCHT, P. V. RANADE and D. P. HARRISON, *ibid.* **43** (1988) 3005.
7. S. K. GANGWAL, J. M. STOGNER and S. M. HARKINS, *Envirn. Progr.* **8** (1989) 26.
8. S. LEW, K. JOTHIMURUGESAN and M. FLYTZANI-STEPHANOPOULOS, *Ind. Engng. Chem. Res.* **28** (1989) 535.
9. S. K. GANGWAL, S. M. HARKINS, M. C. WOODS, S. C. JAIN and S. J. BOSSART, *Envirn. Progr.* **8** (1989) 265.
10. M. C. WOODS, S. K. GANGWAL, D. P. HARRISON and K. JOTHIMURUGESAN, *Ind. Engng. Chem. Res.* **30** (1991) 100.
11. L. N. SA, G. D. FOCHT, P. V. RANADE and D. P. HARRISON, *Chem. Engng. Sci.* **44** (1989) 215.
12. R. GUPTA, S. K. GANGWAL and S. C. JAIN, *Energy and Fuels* **6** (1992) 21.
13. R. E. AYALA and B. M. KIM, *Envirn. Progr.* **8** (1989) 19.
14. S. LEW, A. F. SAROFIN and M. FLYTZANI-STEPHANOPOULOS, *Chem. Engng. Sci.* **47** (1992) 1421.

Received 6 March
and accepted 24 May 1995